Self-oscillating Optical Frequency Comb: Application to Low Phase Noise mm-wave Generation and Radio-over-Fiber Link

G.K.M. Hasanuzzaman, *Student Member, IEEE*, Atsushi Kanno, Pham Tien Dat, and Stavros Iezekiel, *Senior Member, IEEE*

***Abstract*— A self-oscillating optical frequency comb generator (SOFCG) is demonstrated by applying optoelectronic loop feedback to an optical frequency comb generator (OFCG) based on a dual-drive Mach-Zehnder modulator. The resulting SOFCG provides 23 comb lines with a frequency spacing of 11.84 GHz, corresponding to the oscillation frequency defined by the optoelectronic loop. The corresponding OFCG is also implemented by replacing the optoelectronic feedback loop with a microwave synthesizer at 11.84 GHz. A 94.8 GHz mm-wave signal is then generated by selecting two tones and heterodyning in a high speed photodetector for both the SOFCG and the OFCG. The SOFCG system offers superior single sideband phase noise performance compared to the OFCG approach. Using the SOFCG developed here it is possible to generate mm-wave signals up to 260 GHz, and this method is applicable to multiband radio-over-fiber (RoF) links. A radio-over-fiber link is implemented with the SOFCG at 94.8 GHz. An LTE Advanced OFDM FDD 64-QAM signal of 20 MHz bandwidth is transmitted over a 1.3 m wireless distance with an error vector magnitude (EVM) of 2.23%.**

***Index Terms*—Optical frequency comb; Radio-over-fiber; Microwave Photonics.**

I. Introduction

ONE of the most useful attributes of microwave photonics technology is the availability of high bandwidth photodetection, which consequently enables the generation of microwave, mm-wave and THz signals through a variety of topologies and devices [1][2]. This ranges from the use of discrete devices as in mode-locked lasers [3], gain-switched lasers [4], external modulation [5][6], and nonlinear optics [7] to generate optical combs, through to more complex topologies such as optoelectronic oscillators (OEOs) [8] and recirculating optical loops [9]. In all cases the motivation is the feasibility of producing a signal directly in the optical domain, allowing it to be distributed and processed photonically. A key application is in radio-over-fiber (RoF), where the potential of providing multiple carrier frequencies is of interest.

A simple way of generating mm-waves and THz waves is to heterodyne two free running lasers that have a wavelength difference corresponding to the desired frequency spacing [10]. Several RoF links have been demonstrated using this technique [11], but a major limitation is wavelength stability and corresponding frequency and phase fluctuation [4]. Relatively complex and time consuming digital processing is needed for the carrier recovery and phase correction process which increases the overall latency of the system, making it unsuitable for emerging 5G applications. Furthermore, the stability of the generated signal may fail to meet the fluctuation tolerance of the ITU regulation [12][13].

In contrast, the OEO offers the advantage of low phase noise (due to the high-Q conferred by the optical storage element, such as a whispering gallery mode resonator or long optical fiber) and provides outputs in both the RF and optical domain [14], [15]. However, the majority of OEOs have been demonstrated for X-band frequency generation, whereas optical frequency comb generators (OFCGs) can potentially cover THz frequency spans, and through appropriate selection of comb lines can provide multiple frequency outputs [3][4]. Unlike the OEO, however, OFCGs require an external microwave source to both generate the comb and define the comb spacing.

In recent work, the OFCG was embedded in an OEO topology, leading to a self-oscillating frequency comb generator (SOFCG) [16], [17]. The conceptual block diagrams of the OEO, OFCG and SOFCG shown in Fig.1 are compared and contrasted as follows. A SOFCG is essentially an OFCG with optoelectronic feedback: the optical comb is photodetected, producing a microwave output whose fundamental frequency corresponds to the comb spacing, and this fundamental tone is then used to drive the OFCG, thus completing the loop. Hence the resulting SOFCG shares many of the attributes of the OEO (loop oscillation and generation of a microwave output), but whereas the optical portion of the OEO supports only a single wavelength modulated by the microwave oscillation, the SOFCG supports an optical comb. The SOFCG therefore has the advantage of dispensing with an

This project has received funding from the European Union's Horizon 2020 research and innovation programme under the Marie Skłodowska-Curie grant agreement No. 642355. G.K.M Hasanuzzaman also thanks the National Institute of Information and Communication Technology (NICT), Japan for providing a research internship.

G.K.M.Hasanuzzaman and Stavros Iezekiel are with the Microwave Photonics Research Laboratory, EMPHASIS Research Centre, University of Cyprus, Nicosia, 1678, Cyprus (e-mail: ghasan01@ucy.ac.cy, iezekiel@ucy.ac.cy).

Atsushi Kanno and Pham Tien Dat are with the Network System Research Institute, National Institute of Information and Communication Technology, Tokyo 184-8795, Japan (e-mail: kanno@nict.go.jp ptdat@nict.go.jp).

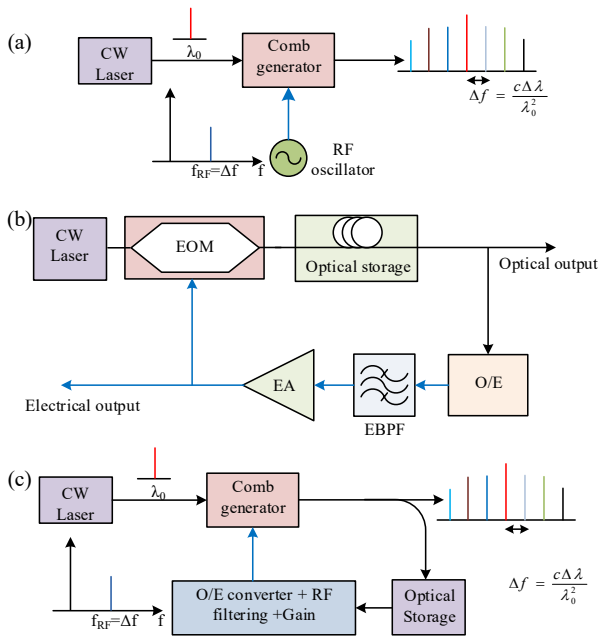

Fig.1 Conceptual block diagram of (a) an optical frequency comb; (b) optoelectronic oscillator; and (c) a self-oscillating optical frequency comb. The optical and electrical paths are represented by the black line and blue line respectively. CW: continuous wave, EOM: electro-optic modulator, EA: electrical amplifier, EBPF: electrical band pass filter.

external microwave source, whilst retaining the low-phase noise attributes of the OEO and the comb generation aspect of the OFCG. Although a conventional OEO could be used to drive a comb generator separately (by connecting the electrical output of the OEO of Fig. 2(b) to the RF port of the comb generator of Fig.2(a)), this would result in the need for more modulators and associated bias circuitry as compared to Fig.2(c), increasing the footprint and cost. In our preliminary work in [18], we implemented an SOFCG based on a dual-loop topology employing a dual-drive Mach-Zehnder modulator and balanced photodetection; up to 23 comb lines with a frequency spacing of 11.84 GHz were produced. Thus a mm-wave signal up to 260.48 GHz can be potentially generated through heterodyning. We also reported the use of a SOFCG to implement a RoF link operating at W-band (94.8 GHz), in which two wavelengths are extracted by a programmable wavelength selective switch (WSS), with modulation being subsequently applied to one wavelength prior to heterodyne photo-detection [18].

In this paper we describe the working principles of the SOFCG, and then measure the phase noise performance of an experimental SOFCG, comparing it with the corresponding OFCG from which it is derived and also with a conventional RF synthesizer. A W-band RoF link is subsequently implemented, allowing a performance evaluation for an LTE-A test signal. We finally indicate an alternative SOFCG topology in which the WSS is integral to the loop, thus avoiding having to photodetect all the tones of the optical comb.

The paper is organized as follows. The fundamental principle of the SOFCG and corresponding analysis are presented in Section II. In Section III, the experimental implementation of a SOFCG and its application to low phase noise mm-wave generation are presented, and compared with a standard OFCG and a commercially-available microwave synthesizer. Section IV outlines the implementation and evaluation of a W-band RoF link using the SOFCG. Finally, in Section V further refinements to the SOFCG topology are described.

II. Self-oscillating Optical Frequency Comb Generator Concept

The self-oscillating optical frequency comb (SOFCG) topology that we use in this work is shown in Fig. 2(a). It is based on an OFCG that employs a dual-drive Mach-Zehnder modulator (MZM) as shown in Fig. 2(b); applying large-signal RF inputs of different amplitudes, a flat comb can be obtained as described in [19]. The optoelectronic feedback loop in Fig.2(a) comprises a dual-loop balanced detection scheme in which a balanced photodetector is fed via a short (L_1) and long (L_2) fiber respectively, an electrical band pass filter (EBPF) for selection of the desired frequency and an electrical amplifier (EA) which along with an erbium-doped fiber amplifier (EDFA) is required to meet the loop gain condition.

By using balanced photo-detection, the impact of RIN from the optical source is reduced, and it has also been shown that this approach reduces the phase noise of microwave photonic links through common mode noise suppression [20][21]. Moreover, the dual-loop configuration is a well-known technique in OEOs, designed to overcome the limitation of a small microwave free spectral range (FSR) that single-loop OEOs suffer from, by applying side-mode suppression [22]. Hence the combination of balanced photodetection and a dual-loop topology helps to minimize the SOFCG phase noise.

Signal analysis based on DDMZM and balanced detection

For the signal analysis we considered the simplified open-loop version of the SOFCG from Fig. 2(a) as illustrated in Fig. 2(c). RF signals of different amplitudes (but identical frequency ω_m) are injected into the two arms of the DDMZM with push-push architecture [23]. The phase shifts induced by the applied RF signals are $S_1(t)= A_1 \cos(\omega_m t)$ and $S_2(t)= A_2 \cos(\omega_m t)$ respectively, the output of the modulator can be expressed as [19]:

$$E_{out} = \frac{1}{2} E_{in}\left[e^{j\theta_1} e^{jA_1\cos\omega_m t} + e^{j\theta_2} e^{jA_2\cos\omega_m t}\right] \quad (1)$$

where $\theta_1=\pi V_{b1}/V_{\pi 1}$ and $\theta_2=\pi V_{b2}/V_{\pi 2}$ are the phase shift induced by the DC bias of arms 1 and 2 respectively; $A_1= \pi V_1/V_{\pi 1}$ and $A_2 = \pi V_2/V\pi_2$ are the modulation indices in which V_1 and V_2 are the amplitudes of the RF drive signals and $V_{\pi 1}$ and $V_{\pi 2}$ are the half-wave voltages of arms 1 and 2 respectively.

The electric fields at the two output ports (E_1 and E_2) of the directional coupler can be expressed by the following equations, considering a 90-degree phase difference between the two ports [24].

$$E_1 = \frac{1}{2\sqrt{2}} E_{in}\left[e^{j\theta_1} e^{jA_1\cos\omega_m t} + e^{j\theta_2} e^{jA_2\cos\omega_m t}\right] \quad (2a)$$

and

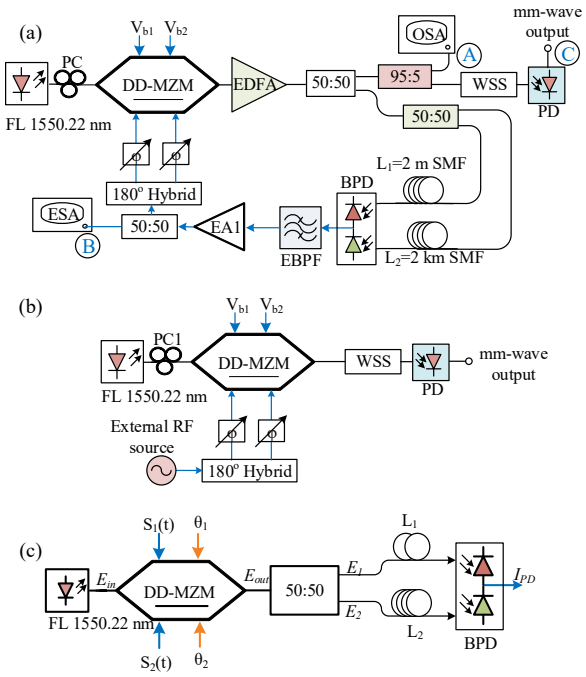

Fig.2 Experimental set-up of: (a) SOFCG; (b) OFCG; (c) Simplified open-loop version of (a) for signal analysis. The optical and electrical paths are represented by black and blue lines respectively. FL: fiber laser, DD-MZM: dual-drive Mach-Zehnder modulator, EDFA: erbium doped fiber amplifier, BPD: balanced photodetector, EBPF: electrical band pass filter, EA: Electrical amplifier, WSS: wavelength selective switch, ESA: electrical spectrum analyzer, OSA: optical spectrum analyzer, PC: polarization controller

$$E_2 = \frac{e^{i\frac{\pi}{2}}}{\sqrt{2}} E_{out} = -\frac{1}{2\sqrt{2}} E_{in}\left[e^{-j\theta_1} e^{jA_1\cos\omega_m t} + e^{-j\theta_2} e^{jA_2\cos\omega_m t}\right] \quad (2b)$$

Assuming the two paths are perfectly balanced (through the use of variable optical attenuators and phase shifters), the corresponding photodetected currents are:

$$I_1 = \Re E_1 E_1^* = \frac{1}{2\sqrt{2}}\Re|E_{in}|^2\left[2 + e^{j(\theta_1-\theta_2)}e^{j(A_1-A_2)\cos\omega_m t} + e^{-j(\theta_1-\theta_2)}e^{-j(A_1-A_2)\cos\omega_m t}\right] \quad (3a)$$

and

$$I_2 = \Re E_2 E_2^* = \frac{1}{2\sqrt{2}}\Re|E_{in}|^2\left[2 + e^{-j(\theta_1-\theta_2)}e^{j(A_1-A_2)\cos\omega_m t} + e^{j(\theta_1-\theta_2)}e^{-j(A_1-A_2)\cos\omega_m t}\right] \quad (3b)$$

where $\Re$ is the responsivity for each photodiode of the BPD (where it is assumed they are identical). Hence the resulting BPD photocurrent is given by:

$$\begin{aligned} I_{PD} &= I_1 - I_2 \\ &= j^2\sqrt{2}\Re|E_{in}|^2\left[\frac{e^{j(\theta_1-\theta_2)} - e^{-j(\theta_1-\theta_2)}}{2j}\right]\cdot \\ &\left[\frac{e^{j(A_1-A_2)\cos\omega_m t} - e^{-j(A_1-A_2)\cos\omega_m t}}{2j}\right] \\ &= -\sqrt{2}\Re|E_{in}|^2[\sin(\theta_1-\theta_2)\sin((A_1-A_2)\cos\omega_m t] \end{aligned} \quad (4)$$

Upon filtering by the bandpass filter, the first-order term in (4) is selected:

$$I_{PD} = -2\sqrt{2}\Re|E_{in}|^2\sin(2\Delta\theta)J_1(2\Delta A)\cos\omega_m t \quad (5)$$

where $\Delta A = (A_1 - A_2)/2$ and $\Delta\theta = (\theta_1 - \theta_2)/2$. From eq. (5) we find that I_{PD} is maximized when $\Delta\theta = \pi/4$ which is also the condition of maximum conversion efficiency for ultra-flat comb generation [19].

III. Experimental Implementation of SOFCG

A. Experimental setup

The SOFCG depicted in Fig.2(a) was evaluated experimentally. A fiber laser (FL) of 15 Hz linewidth and 13 dBm output power at 1550.22 nm was used as a continuous-wave (CW) optical source for the DDMZM. The DDMZM functions both as the E/O converter for the optoelectronic loop and as a frequency comb generator as described in the previous section. The output of the DDMZM was then amplified by an erbium-doped fiber amplifier (EDFA) and split into two paths by a 50:50 coupler, with one being used to form the loop. The other was diverted (via a 95:5 coupler which was used to monitor the optical spectrum at point **A** with a Yenista Optics OSA-20 optical spectrum analyzer) to the optical output of the SOFCG.

Short and long fiber lengths of L_1 = 2 m and L_2 = 2 km respectively were used to feed a balanced photodiode (Finisar BPDV2150R, with a 3-dB bandwidth of 43 GHz and responsivity of 0.45 A/W). A microwave band pass filter (EBPF) (Tamagawa SBF-203 BPF with a 3-dB bandwidth of 300 MHz) was used to select the desired RF signal, which was subsequently amplified by a low noise amplifier (SHF 806E with 26 dB gain) prior to a RF power splitter, one output of which was connected to the RF port of the DDMZM to close the SOFCG loop and the other to an electrical signal analyzer (Agilent N9030A PXA) at point **B** for monitoring the spectrum and measuring the phase noise performance.

In addition, by selecting any two comb lines at the optical output of the SOFCG it is possible to generate (through heterodyning in a photodiode with sufficiently high bandwidth) mm-wave signals of integral multiples of the comb frequency spacing. By placing a programmable wavelength selective switch (Finisar WaveShaper 16000S) immediately after the optical output of the SOFCG, we selected two lines in order to generate the corresponding mm-wave signal at the output of a high speed photodiode (Finisar XPDV4120R) as indicated by point **C** in Fig. 2(a).

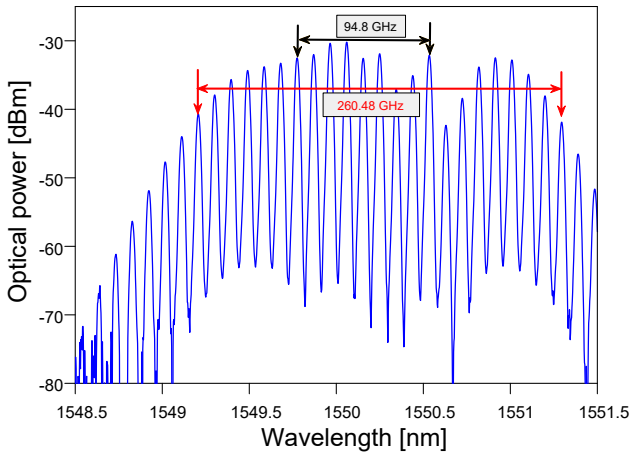

Fig. 3. Optical spectrum of the generated optical frequency comb with a frequency spacing of 11.84 GHz at the center wavelength of 1550.22 nm (measured with an OSA at point **A** in Fig. 2(a))

B. SOFCG results for RF signal generation

The optical spectrum of the generated comb lines from the SOFCG (as taken from point **A** in Fig. 2(a)) is shown in Fig. 3; the comb spacing is 11.84 GHz, with 23 comb lines being generated considering approximately 12 dB deviation from the peak. In this preliminary proof-of-concept work, comb flatness was not prioritized, given that the end application was mm-wave RoF (as will be described in §IV). The electrical spectrum of the corresponding 11.84 GHz signal (measured at point **B** in Fig. 2(a)) is shown in Fig.4. This frequency is determined by the dual-loop fiber topology of the SOFCG and the passband of the EBPF. A side mode suppression ratio of 60 dB was obtained with the balanced detection based dual-loop configuration, as shown in Fig. 4(b). In addition, the single side band (SSB) phase noise of the generated RF

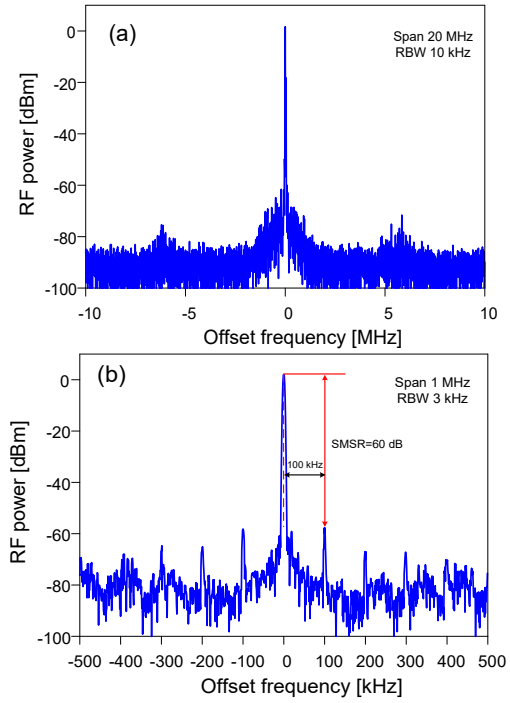

Fig. 4. Electrical spectrum of the 11.84 GHz signal. (a) Span 20 MHz, RBW 10 kHz (b) Span 1 MHz, RBW 3 kHz. A side mode suppression ratio of 60 dB has been obtained.

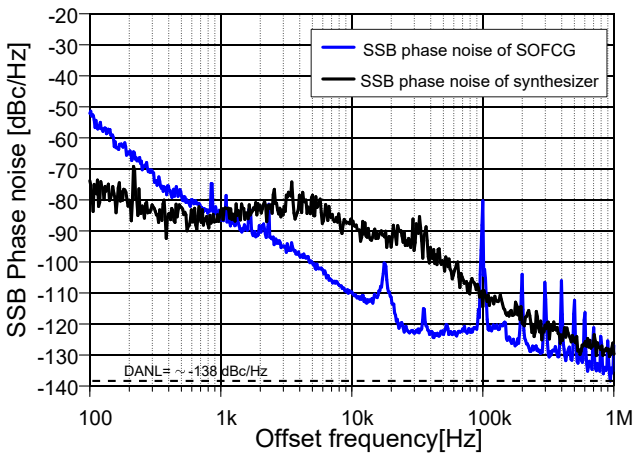

Fig. 5. SSB phase noise of the 11.84 GHz oscillation measured at point **B** for the SOFCG (blue line) and of an HP 83620A synthesizer (black line).

oscillation at point **B** was measured using the phase noise measurement functionality of the signal analyzer, and this is compared with a commercial microwave synthesizer set to an oscillation frequency of 11.84 GHz (HP 83620A) (the best available in our laboratory in terms of phase noise) in Fig. 5. The phase noise of the SOFCG is lower than the HP synthesizer beyond the 1 kHz offset. The SSB phase noise of the 11.84 GHz signal at a 10 kHz offset is 22 dB lower for the SOFCG (-110 dBc/Hz) than for the HP 83620A (-88 dBc/Hz). Table I compares and contrasts some recently reported SOFCGs in terms of optical bandwidth, number of comb lines, comb spacing and phase noise. As indicated in Table I, our proposed system provides a wider optical bandwidth with typical phase noise than other recently reported results. Additionally, [8] used two modulators (cascading of a DD-MZM with a PM) while our system requires only one modulator (DD-MZM)

Table I: Compares and contrasts recently reported SOFCGs with the SOFCG demonstrated here.

Ref.	Optical bandwidth	Comb lines	Comb spacing	Phase noise @ 10 kHz
[16]	120 GHz	13	9.95 GHz	-78 dBc/Hz
[8]	160 GHz	17	10 GHz	-122 dBc/Hz
	156 GHz	14	12 GHz	-115 dBc/Hz
[17]	144 GHz	13	12 GHz	Not available
	120 GHz	13	10 GHz	-101 dBc/Hz
[28]	86 GHz	9	10.89 GHz	-93 dBc/Hz
Proposed work	260 GHz	23	11.84 GHz	-110 dBc/Hz

C. Low phase noise mm-wave generation using SOFCG and comparison with OFCG- and RF synthesizer based approaches

Using the wavelength selective switch for the SOFCG, we selected two lines spaced eight intervals apart (Fig. 6(a)) in order to generate a 94.8 GHz signal (Fig. 6(b)) at the output of the high speed photodiode (point **C** in Fig. 2(a)) and then measured the SSB phase noise.

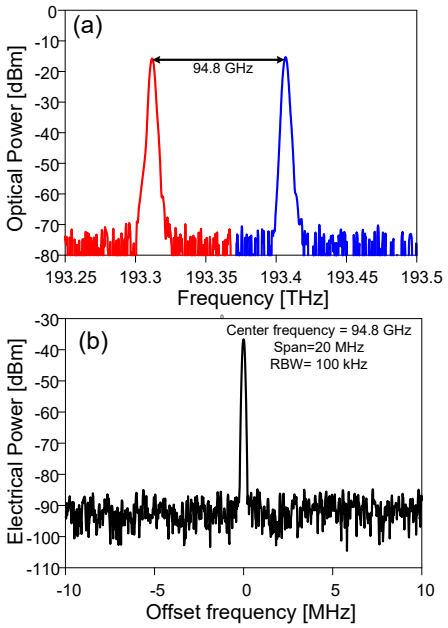

Fig. 6. (a) Optical spectrum of two tone signal with spacing of 94.8 GHz (b) The electrical spectrum of the generated 94.8 GHz oscillation

We then proceeded to compare the phase noise performance of the SOFCG with that of the corresponding OFCG shown in Fig. 2(b), in order to verify the superiority of the former method. In this case the OFCG was driven by an HP 83620A synthesizer at 11.84 GHz, with the WSS again set to filter out two comb lines spaced eight intervals apart so as to generate a 94.8 GHz signal.

In addition to direct generation of the 94.8 GHz signal through use of the WSS and heterodyning, it is also possible in principle to use electronic frequency multiplication of the SOFCG's RF oscillation frequency. With this approach, a frequency multiplier would be placed at point **B** in Fig. 2(a), with a multiplication factor set to eight. However, when a reference microwave signal is multiplied by N, the phase noise is degraded by 20 $\log_{10} N$, which for a factor eight results in an additional 18 dB penalty. We therefore used this and the measured results from Section III B in order to estimate the

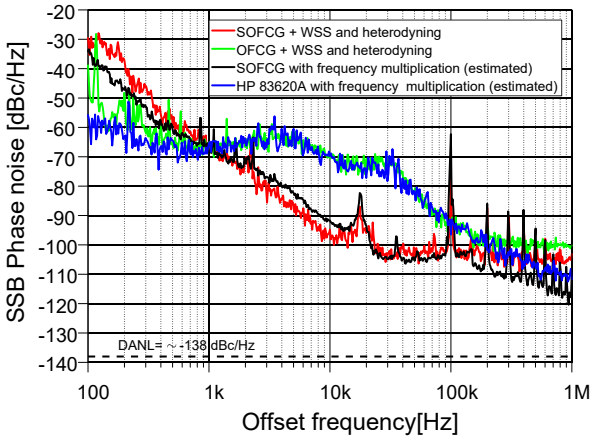

Fig. 7. Measured SSB phase noise of: 94.8 GHz signal generated using SOFCG (red line); 94.8 GHz signal generated using conventional OFCG (green line). Estimated SSB phase noise of the 94.8 GHz signal using SOFCG and multiplication (black line) and of the 94.8 GHz signal using a synthesizer and multiplication (blue line).

Table II: SSB phase noise (dBc/Hz) performance at 94.8 GHz for the SOFCG and OFCG using WSS and heterodyning (measured) and using electronic multiplication (×8) of the 11.84 GHz signal from the OFCG and RF synthesizer (estimated).

SSB Phase Noise (dBc/Hz)	Offset frequency			
	100 Hz	1 kHz	10 kHz	100 kHz
SOFCG + WSS and heterodyning	-32.01	-65.92	-96.99	-101.06
SOFCG with frequency multiplication (estimated)	-33.55	-66.04	-92.09	-101.46
OFCG + WSS and heterodyning	-45.87	-66.68	-69.66	-92.68
HP 83620A with frequency multiplication (estimated)	-58.92	-66.01	-70.50	-92.01

phase noise performance of the SOFCG and HP 83620A synthesizer when electronic multiplication is used instead of comb selection and heterodyning.

The comparison between the SOFCG, the OFCG, and the RF synthesizer for the SSB phase noise performance at 94.8 GHz is shown in Fig.7 and also summarized in Table II for both the WSS-heterodyning approach and the electronic multiplication method. From Fig.7 and Table II it is seen that the SOFCG-based mm-wave generation using heterodyning of the comb lines performs better than the other approaches. The SSB phase noise of this method is 27 dB better than the conventional OFCG based approach at an offset frequency of 10 kHz. The improvement is intrinsically due to the SOFCG topology, which in a similar way to OEO topologies can provide optoelectronic oscillation of high spectral purity inside the loop.

IV. SOFCG-Based Radio-Over-Fiber Link

A. Experimental setup

We developed a 94.8 GHz RoF link based on the SOFCG arrangement of Fig. 2(a). The proof-of-concept experimental set-up is illustrated in Fig. 8. The two-tone optical signal

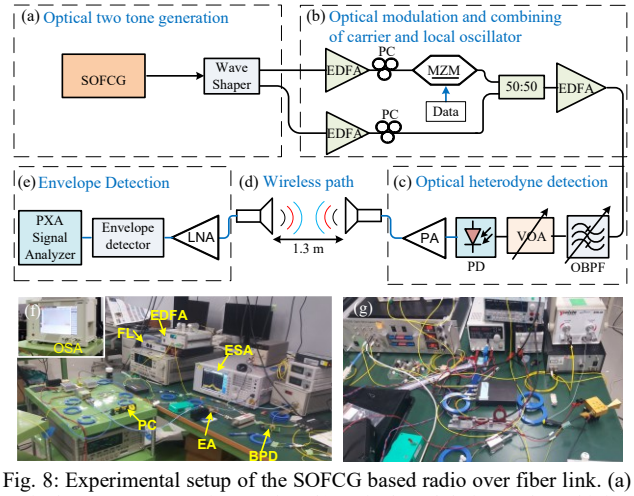

Fig. 8: Experimental setup of the SOFCG based radio over fiber link. (a) optical two tone generation section (b) optical modulation and combining of carrier and local oscillator (c) optical heterodyning in high speed photodetector (d) wireless section (e) envelope detection section (f) photo of optical modulation and heterodyning section (g) photo of SOFCG. The SOFCG block consists of the arrangement in Fig. 2(a).

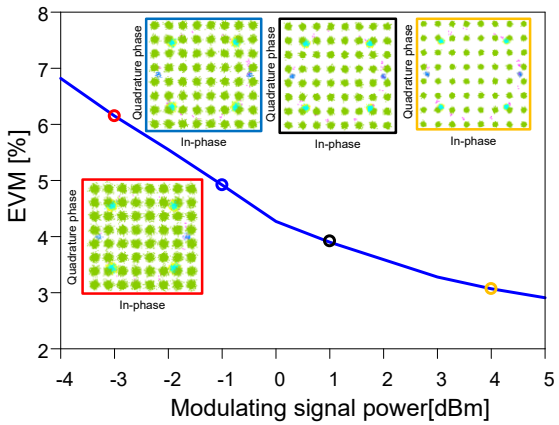

Fig.9: EVM vs modulating signal power of the transmission system. The insets are the constellation diagram for a 64 QAM OFDM signal over a 1.3 m wireless transmission path. The frame color of the constellation diagrams corresponds to the dot points in the line plot.

required for heterodyning in order to generate the mm-wave carrier was obtained from the SOFCG (Fig. 8(a)) using the techniques described in § III. A Finisar WaveShaper 16000S was used to select two comb lines (separated by 94.8 GHz) and route them into two different output ports. One of these outputs was routed through a MZM for data modulation as shown in Fig. 8(b); we used an Agilent PSG vector signal generator (E8267D) to generate a LTE-A standard downlink signal centered at 1 GHz with a bandwidth of 20MHz and modulation format 64 QAM. The modulated comb line was combined with the other comb line. The combined optical signal was then amplified by an EDFA; filtered by a 1 nm tunable optical band pass filter to remove the out-of-band amplified spontaneous emission (ASE); and adjusted by a variable optical attenuator (VOA) to control the input optical power before heterodyning in a high speed photodiode (Finisar XPDV4120R) as shown in Fig. 8(c). The output of the photodetector was amplified by a power amplifier (PA). The amplified signal was connected to a horn antenna with a gain of 23 dBi (at 95 GHz) and propagated over a 1.3 m wireless link. A second identical horn antenna placed in the same polarization was used to receive the radiated signal. The received W band signal was then amplified by a low noise amplifier (LNA), down converted by an envelope detector and analyzed by a vector signal analyzer (Agilent N9030A PXA). A Schottky barrier diode (SBD) was used as the envelope detector.

B. Results and discussion

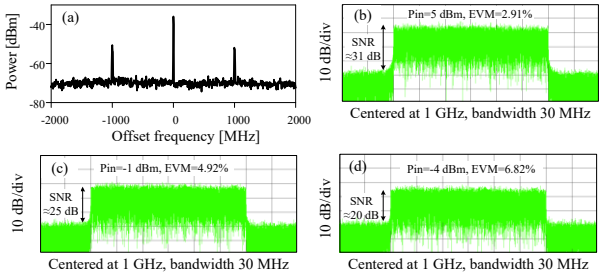

Fig.10. (a) DSB modulated data signal (b)-(d) Electrical spectrum of the demodulated signal for different modulating power condition. EVM decreases with the increment of modulating power due to the increment of signal to noise ratio (SNR).

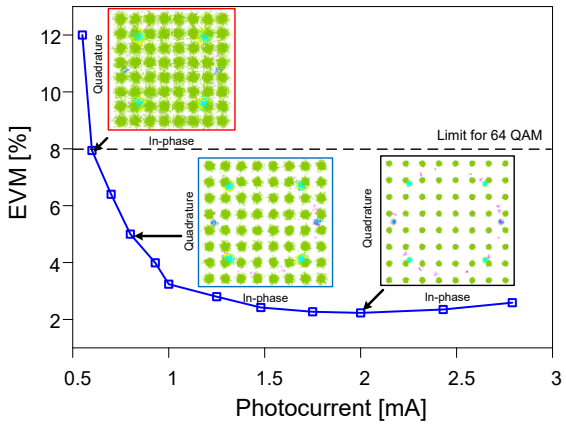

Fig.11: EVM vs photocurrent of the SOFCG based RoF system. The insets are the constellation diagram of (64 QAM OFDM signal, 1.3 m wireless transmission distance).

The effect of modulating signal power (P_{in}) on the error vector magnitude (EVM) under varying modulating signal power is depicted in Fig. 9 for a LTE-A 64 QAM signal transmitted over a 1.3 m wireless distance. The modulating signal power was varied from -4 dBm to 5 dBm and we found that the EVM is reduced for higher modulating signal powers. This is due to the fact that increasing modulating power enhances the SNR of the signal, resulting in a low EVM as shown in Fig.10 (b)-(d). A variable optical attenuator in front of the photodiode was then used to adjust the incident optical power and hence the generated I_P. The measured EVM as a function of photocurrent (I_P) is illustrated in Fig. 11 for a LTE-A 64 QAM signal transmitted over a 1.3 m wireless distance. The lowest obtained EVM is 2.23% at I_P = 2 mA. For values of I_P above 2 mA, the EVM increases due to the saturation effect in the amplifier stage at the receiver. The measured EVM is degraded by 45% for a 50% reduction of I_P. The insets show the corresponding constellation diagrams. The measured EVM is within the limit of 8% for 64 QAM [25][26] for the photocurrent above I_p=0.6 mA.

V. SOFCG With Integral Wavelength Selection

A simple modification to the SOFCG tropology described in §II is illustrated in Fig.12, whereby the WSS is now incorporated within the optoelectronic loop instead of being located after the SOFCG optical output. In this way, rather than all the comb lines being applied to the BPD, the WSS selects two tones corresponding to the RF oscillation frequency of the SOFCG which then are routed to the BPD via the 50:50 coupler and the fibres L_1 and L_2, and a further two

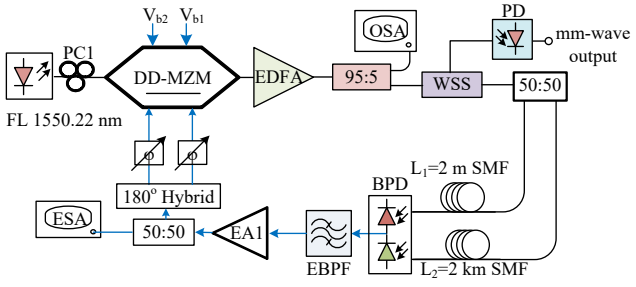

Fig.12. The modified configuration of Fig.2(a) as SOFCG where the WSS is included inside the OEO loop.

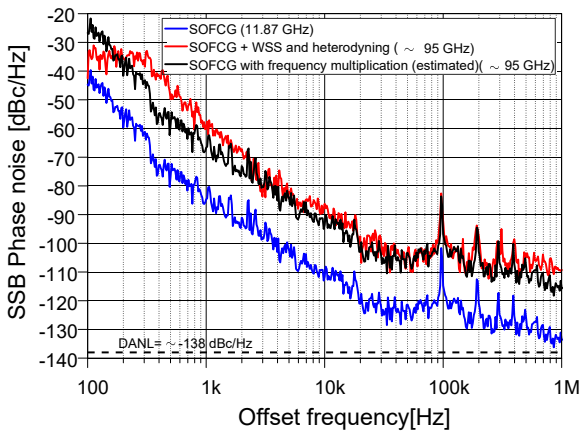

Fig. 13. SSB phase noise of the 11.87 GHz oscillation obtained by modified SOFCG (blue line) and of the 95 GHz oscillation obtained from optical heterodyning (red line), along with estimated SSB phase noise (black line) assuming ×8 frequency multiplication of the 11.87 GHz output.

tones which are routed to the other output of the WSS in order to generated the desired mm-wave output. Typical phase noise performance is shown in Fig.13, which is comparable to the performance of the SOFCG results shown in Fig.5 and Fig.7. Further results from this approach will be reported in [27].

VI. Conclusions

We have demonstrated a self-oscillating frequency comb generator that combines the advantages of a conventional optical frequency comb with those of an optoelectronic oscillator, namely generation of a stable optical comb allowing mm-wave signals to be synthesized, along with the low phase noise characteristics that are typical of OEOs. The SOFCG provides 23 comb lines with 11.84 GHz spacing that can potentially generate mm-waves up to 260 GHz. The phase noise performance of an SOFCG with a loop oscillation frequency of 11.84 GHz was compared and contrasted with that of a conventional microwave synthesizer, and the phase noise performance when used to generate a 94.8 GHz signal either through optical heterodyning or electronic multiplication was also evaluated. The SSB phase noise of the 11.84 GHz oscillation is -110 dBc/Hz at a 10 kHz offset, while for the 94.8 GHz output it is -97 dBc/Hz at a 10 kHz offset.

The SOFCG was then used to implement a W-band radio-over-fiber link, in which an LTE Advanced standard 64 QAM signal was sent over a wireless path of 1.3 m with an EVM as low as 2.35%. Finally, we have indicated how the SOFCG topology may be potentially modified via the inclusion of the wavelength selective switch within the optoelectronic loop of the SOFCG, without adversely affecting phase noise performance.

References

[1] J. P. Yao, "Microwave Photonics," *J. Light. Technol.*, vol. 27, no. 3, pp. 314–335, 2009.

[2] J. Yao, "A Tutorial on Microwave Photonics," *Photonics Soc. Newsl.*, vol. 24, no. April, pp. 4–12, 2012.

[3] S. Koenig *et al.*, "Wireless sub-THz communication system with high data rate," *Nat. Photonics*, vol. 7, pp. 977–981, 2013.

[4] H. Shams *et al.*, "100 Gb/s multicarrier THz wireless transmission system with high frequency stability based on a gain-switched laser comb source," *IEEE Photonics J.*, vol. 7, no. 3, 2015.

[5] J. K. Hmood, S. D. Emami, K. A. Noordin, H. Ahmad, S. W. Harun, and H. M. H. Shalaby, "Optical frequency comb generation based on chirping of Mach-Zehnder Modulators," *Opt. Commun.*, vol. 344, pp. 139–146, 2015.

[6] T. Kawanishi, T. Sakamoto, and A. Kanno, "Sub-THz radio-over-fiber signal generation using external modulation," *EICE Electron. Express*, vol. 12, no. 13, pp. 1–12, 2015.

[7] D. Hillerkuss *et al.*, "High-quality optical frequency comb by spectral slicing of spectra broadened by SPM," *IEEE Photonics J.*, vol. 5, no. 5, 2013.

[8] J. Dai *et al.*, "Self-oscillating optical frequency comb generator based on an optoelectronic oscillator employing cascaded modulators," *Opt. Express*, vol. 23, no. 23, p. 30014, 2015.

[9] A. Kanno and T. Kawanishi, "Phase noise analysis of an optical frequency comb using single side-band suppressed carrier modulation in an amplified optical fiber loop," *IEICE Electron. Express*, vol. 9, no. 18, pp. 1473–1478, 2012.

[10] S. Iezekiel, *Microwave photonics: devices and applications*. Wiley, 2009.

[11] H. Shams, M. J. Fice, K. Balakier, C. C. Renaud, F. van Dijk, and A. J. Seeds, "Photonic generation for multichannel THz wireless communication.," *Opt. Express*, vol. 22, no. 19, pp. 23465–72, 2014.

[12] Rec. ITU-R SM.1045-1, "Frequency tolerance of transmitters." [Online]. Available: http://www.itu.int/rec/R-REC-SM.1045-1-199707-I. [Accessed: 15-Nov-2017].

[13] A. Kanno *et al.*, "Evaluation of frequency fluctuation in fiber-wireless link with direct IQ down-converter," in *European Conference on Optical Communication, ECOC*, 2014, pp. 6–8.

[14] X. S. Yao and L. Maleki, "Optoelectronic microwave oscillator," *J. Opt. Soc. Am. B*, vol. 13, no. 8, p. 1725, 1996.

[15] L. Maleki, "The optoelectronic oscillator," *Nat. Photonics*, vol. 5, no. December, pp. 728–730, 2011.

[16] T. Sakamoto, T. Kawanishi, and M. Izutsu, "Optoelectronic oscillator using a LiNbO3 phase modulator for self-oscillating frequency comb generation.," *Opt. Lett.*, vol. 31, no. 6, pp. 811–3, Mar. 2006.

[17] M. Wang and J. Yao, "Tunable optical frequency comb generation based on an optoelectronic oscillator," *IEEE Photonics Technol. Lett.*, vol. 25, no. 21, pp. 2035–2038, 2013.

[18] G. K. M. Hasanuzzaman, A. Kanno, P. T. Dat, and S. Iezekiel, "W-band radio-over-fiber link based on self-oscillating optical frequency comb generator," in *Optical Fiber Communication Conference*, 2018, p. paper W1F.6.

[19] T. Sakamoto, T. Kawanishi, and M. Izutsu, "Asymptotic formalism for ultraflat optical frequency comb generation using a Mach-Zehnder modulator.," *Opt. Lett.*, vol. 32, no. 11, pp. 1515–1517, 2007.

[20] J. Hu, Y. Gu, W. Tan, W. Zhu, L. Wang, and M. Zhao, "Microwave photonic link with improved phase noise using a balanced detection scheme," *Opt. Commun.*, vol. 370, pp. 1–5, 2016.

[21] C. Jiang, W. Zou, H. Zhang, and J. Chen, "Improvement of phase noise in a widely tunable optoelectronic oscillator based on balanced detection," in *2015 Opto-Electronics and Communications Conference, OECC 2015*, 2015, pp. 1–3.

[22] X. S. Yao and L. Maleki, "Multiloop optoelectronic oscillator," *IEEE J. Quantum Electron.*, vol. 36, no. 1, pp. 79–84, 2000.

[23] T. Asakura *et al.*, *High-Order Modulation For Optical Fiber*. Berlin: Springer, 2009.

[24] R. März, *Integrated optics : design and modeling*. Boston: Artech House, 1994.

[25] 3GPP TS36.104 V10.9.0 Releasee 10, "Evolved Universal Terrestrial Radio Access (E-UTRA);Base Station (BS) radio transmission and reception," 2013. [Online]. Available: http://www.3gpp.org/dynareport/36-series.htm.

[26] A. Kanno, P. T. Dat, N. Sekine, I. Hosako, and T. Kawanishi, "High-Speed Coherent Transmission Using Advanced Photonics in Terahertz Bands," no. 12, pp. 1071–1080, 2015.

[27] A. Kanno, G. K. M. Hasanuzzaman, N. Yamamoto, and S. Iezekiel, "Optical frequency comb applied optoelectronic oscillator for millimeter-wave signal generation and its application," in *SPIE Defense and Security, Passive and Active Millimeter-Wave Imaging XXI*, p. paper 10634-13.

[28] J. Liu, B. Zheng, C. Shu, and S. Member, "Self-Oscillating Optical Frequency Comb Based on a Raman-Pumped Brillouin Optoelectronic Oscillator," *IEEE Photonics J.*, vol. 29, no. 12, pp. 1003–1006, 2017.